Macromolecules

pubs.acs.org/Macromolecules Article

Effect of Changing Interfacial Tension on Fragmentation Kinetics of Block Copolymer Micelles

Supriya Gupta and Timothy P. Lodge*

Cite This: https://doi.org/10.1021/acs.macromol.2c02158 Read Online

ABSTRACT: Micelle fragmentation, one of the key mechanisms responsible for equilibration of kinetically trapped micelles, is investigated for block copolymer micelles in ionic liquids (ILs). In particular, the role of driving force for micelle fragmentation is studied by altering the solvent quality after micelle preparation, amounting to a jump in interfacial tension γ between solvent and the micelle core. Direct dissolution of a 1,2-polybutadiene-*b*-poly(ethylene oxide) (PB-*b*-PEO) copolymer (M_n = 17.5 kDa and f_{PEO} = 0.38) in the ionic liquid [C_2mim][TFSI] results in large micelles with average size $\langle R_h \rangle_\circ \approx$ 68 nm and dispersity $Đ \approx$ 1.27. The solution of the as-prepared micelles is then diluted by the careful addition of a second ionic liquid [C_{10}mim][TFSI] having lower γ with the micelle core, such that the micelles remain unaffected. The γ and hence the quality of the solvent mixture were controlled by the degree of dilution. The choice of the second solvent is based on the measurement of γ for a series of [$C_x$mim][TFSI] ILs with 1-2-polybutadiene homopolymer, carried out using a pendant drop test. Diluting the micelles by adding another ionic liquid with lower γ tends to decrease the equilibrium micelle size, which, in turn, enhances the driving force for fragmentation of the bigger as-prepared micelles, represented by increase in the ratio of aggregation numbers Q/Q_{eq}. Subjecting the diluted micellar solution to temperature-jump to 170 °C followed by thermal annealing leads to fragmentation of the as-prepared micelles to attain a near-equilibrium state. The micelles are characterized using an in situ dynamic light scattering (DLS) technique to observe the time evolution of average micelle size, from which the relaxation time is obtained. Additionally, small-angle X-ray scattering (SAXS) and cryogenic transmission electron microscopy (TEM) measurements were carried out to obtain the micelle core size and distribution in the micellar solutions before and after fragmentation. The enhancement in the driving force achieved by controlling the amount of low γ solvent resulted in faster fragmentation; the characteristic fragmentation time decreases monotonically on increasing the size ratio Q/Q_{eq} from 1.2 to 5.

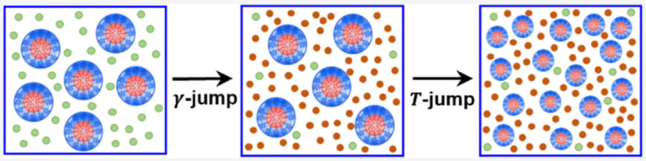

■ INTRODUCTION

Block copolymers (BCPs) are fascinating materials due to their ability to self-assemble into a myriad of nanostructures, both in bulk[1] and solution.[2−4] Many studies, both experimental as well as computational, have revealed the rich self-assembly behavior of BCPs.[5−10] The enthalpic energy arising from chemical dissimilarity of the constituent blocks coupled with the conformational entropy of the polymeric chains governs the eventual organization. In particular, spherical micelles with a core-shell structure have been gaining significant attention as a universal carrier for targeted drug delivery.[11,12] In addition to nanomedicine, BCP micelles find practical interest in many biological and industrial applications, such as nanoreactors, in nano-templating, as imaging agents, and as viscosity modifiers for motor oil.[13−16] In solution, the contrast in selectivity of the blocks toward the solvent imparts an amphiphilic character responsible for micellization, and the choice of solvent plays a key role. Careful control of molecular weight, block composition, and chain architecture together with the nature of solvent, temperature, concentration, method of preparation, and addition of homopolymers or ions can provide a variety of micelle structures, such as spheres, worms, vesicles, and bicontinuous structures.[17−21] Concurrently, ionic liquids (ILs) are receiving increasing attention due to their extraordinary physicochemical properties, such as thermal and chemical stability, high temperature windows, and negligible vapor pressure, and tunable cohesive energy density. The use of ILs as solvents for micellization of BCPs was first explored by He et al.[22]

While the equilibrium micellar structures attained via self-assembly are relatively well studied, the understanding of the micelle formation and their equilibration processes is still incomplete.[23,24] To realize the full potential of BCP micelles, an extensive understanding of the dynamics of micelle formation and equilibration processes is essential to optimize structure−property relationships. The equilibration of surfactant micelles has been studied extensively.[25−27] For BCP micelles, theoretical description of the equilibration mechanism[28−30] is supported by

Received: October 21, 2022
Revised: January 28, 2023

a few experimental studies which generally focus on a single mechanism in isolation, such as chain exchange,[31−41] or fusion and fragmentation.[42,43] A comprehensive review of the dynamics and equilibration of BCP micelles along with the future scope and challenges has been presented in a recent review.[44]

For BCP micelles that are significantly larger/smaller than the equilibrium size, the relaxation toward equilibrium state is governed predominantly by fragmentation/fusion mechanisms, neither of which has been studied extensively. Previous studies estimated the rate constants for the fragmentation and fusion processes for poly(ethylene oxide)-*b*-poly(propylene oxide)-*b*-poly(ethylene oxide) triblock copolymer micelles using fluorescence decay methods.[42] It was found that for micelles near equilibrium, the rates for fragmentation and fusion processes are on the order of 10^6 times slower than chain exchange. Recent experiments showed that variation in the length of the triblock copolymers can greatly affect the fragmentation kinetics.[43]

Experimental studies on the relaxation of as-prepared micelles far from the equilibrium state are limited. For such a study, one needs to prepare micelles that are either significantly smaller or much larger than the equilibrium size in order to capture the regimes of fusion or fragmentation processes, respectively. Eisenberg et al. proposed an interesting approach to prepare micelles of different sizes from a single BCP by altering the sample preparation method.[45−47] Following this protocol, Meli et al. used direct dissolution method to prepare micelles of 1,2-polybutadiene-*b*-poly(ethylene oxide) (PB-*b*-PEO) in imidazolium-based ILs, such as 1-ethyl-3-methylimidazolium bis(trifluoromethylsulfonyl)imide ([C_2mim][TFSI]) and 1-butyl-3-methylimidazolium bis(trifluoromethylsulfonyl)imide ([C_4mim][TFSI]).[48,49] The authors observed that the direct dissolution method produces micellar aggregates significantly larger than the equilibrium size ($Q/Q_{eq} > 1.5$) where Q and Q_{eq} denote the aggregation numbers for the as-prepared micelles and the equilibrium micelles, respectively. The kinetically trapped as-prepared micelles can be driven toward the equilibrium state under external stimuli, the most common being a temperature-jump. Large micelles were subjected to relaxation upon thermal annealing at an elevated temperature (e.g., 170 °C). During relaxation, the time evolution of average micelle size and distribution were followed using dynamic light scattering (DLS), small-angle X-ray scattering (SAXS), and transmission electron microscopy (TEM) techniques, all of which gave consistent results. Irrespective of the annealing temperature, the decay of micelle size was found to be well described by a compressed exponential form with an "Avrami" exponent $n \approx 2$. The study provided an estimate of the characteristic relaxation time τ. Since time-resolved small-angle neutron scattering experiments on the same system revealed no chain exchange up to at least 200 °C, the observed relaxation time during annealing at 170 °C is presumed to be dominated by fragmentation. Recently, Early et al. conducted experiments on PB-*b*-PEO micelles in different ILs and employed DLS, SAXS, and TEM to clearly identify the roles of various factors influencing the rate of micelle fragmentation.[50,51] Fragmentation being a first-order process, the rate of fragmentation was found to be independent of micellar concentration. Interestingly, the fragmentation time was reported to be independent of the solvent quality and, therefore, interfacial tension γ, which suggests that the barrier to fragmentation does not involve exposure of micelle core to the surrounding solvent. It should be noted that micelles were prepared and relaxed in the same solvent and the experiments were performed in a series of solvents to vary the solvent quality. The authors also report a strong dependence of fragmentation rate on BCP molecular weight, consistent with the theoretical prediction of Dormidontova.[30] The influence of altering the solvent quality on structure and chain exchange kinetics in BCP micelles has also been investigated extensively.[40,52−56]

Recent studies have captured the morphological transition from cylindrical to spherical micelles using time-resolved small-angle neutron (TR-SANS) and X-ray scattering (TR-SAXS).[57,58] Direct imaging of fusion and fragmentation events provides unique insight into the evolution of micellar structures and their characteristics.[59,60] Recently, time-resolved TEM imaging of BCP micelles in ILs depicted the evolution of micellar morphology during fragmentation.[61] The TEM imaging indicated a sequential transition from a spherical micelle to a prolate spheroid, then to a "peanut-shaped" micelle followed by the creation of two micelle cores with overlapping coronas, and finally to detachment of coronas to generate two spherical micelles. Similar events were reported earlier by Gao et al. using the dissipative particle dynamics (DPD) simulations.[62]

The present study is aimed at understanding the effect of micelle size ratio Q/Q_{eq}, an indication of the departure of as-prepared micelles from equilibrium, on the kinetics of fragmentation. The methodology adopted in the prior studies does not allow controlled variation of Q/Q_{eq} over a broad range, and thus the value was fixed, typically ≈ 1.5−2. Here, we adopt a new sample preparation methodology, which allows us to vary Q/Q_{eq} significantly, by altering the solvent quality after micelle preparation. Micelles are first prepared in a solvent with higher γ followed by dilution with the second solvent with a lower γ value. The choice of the solvents was made based on direct measurements of γ between the solvent and a PB homopolymer. The diluted micellar solution is then subjected to high-temperature annealing to attain equilibration. Dilution by a low γ solvent leads to reduction in equilibrium micelle size (Q_{eq}), which in turn increases the ratio Q/Q_{eq}. Micelle sizes before and after fragmentation are characterized by in situ DLS, SAXS, and TEM.

■ EXPERIMENTAL SECTION

Synthesis and Characterization. A PB-*b*-PEO sample was synthesized previously via a two-step sequential anionic polymerization.[51] The resulting PB-*b*-PEO diblock copolymer is denoted as BO(9−8), where the numbers in parentheses refer to the number-average molecular weight of each block in kDa. Size exclusion chromatography (SEC) with multiangle light scattering detection (Wyatt Instruments DAWN) was used to obtain the molecular weight (M_n) and the dispersity ($Đ$). ^{1}H nuclear magnetic resonance spectroscopy using a Varian Inova 500 spectrometer was performed in $CDCl_3$ to calculate the polymer block composition. For BO(9−8), the total M_n = 17.5 kDa and $Đ$ = 1.10, with $M_{n,PB}$ = 8.6 kDa, $M_{n,PEO}$ = 7.8 kDa, and f_{PEO} = 0.38. The homopolymer 1,2-polybutadiene (PB) used for γ measurements was also synthesized previously using anionic polymerization with M_n = 4.7 kDa and $Đ$ = 1.10. The ILs 1-ethyl-3-methylimidazolium bis(trifluoromethylsulfonyl)imide 99% ([C_2mim][TFSI]) and 1-decyl-3-methylimidazolium bis(trifluoromethylsulfonyl)imide 99% ([C_{10}mim][TFSI]) were purchased from IoLiTec. ILs were dried under vacuum (<100 mTorr) at 60 °C for 60 h prior to use and were characterized by ^{1}H NMR spectroscopy in DMSO-d_6. The NMR spectra and SEC chromatograms for both polymers and ILs are provided in the Supporting Information, Figures S1−S5.

https://doi.org/10.1021/acs.macromol.2c02158
Macromolecules XXXX, XXX, XXX−XXX

Interfacial Tension Measurement. The interfacial tension γ between the solvent and the core-forming polymer block plays an important role in controlling the size of the micelles at equilibrium. Tuning γ, therefore, alters the equilibrium aggregation number of the micelles (Q_{eq}), which, in turn, controls the size ratio (Q/Q_{eq}) where Q is the mean aggregation number of the micelles. Thus, by varying γ of an as-prepared micellar solution, one can alter the ratio Q/Q_{eq} and study the effect of the thermodynamic driving force on the rate of fragmentation. The γ between PB, which forms the core of the block copolymer micelles, and different ILs was measured using a Kruss DSA-30S tensiometer using the pendant drop technique in which a drop of ionic liquid is suspended in a reservoir of PB homopolymer at 70 °C. A schematic of a pendant drop profile is presented in Figure 1. Once

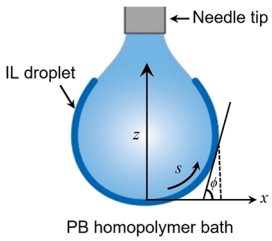

Figure 1. Schematic diagram depicting a typical pendant drop profile.

stabilized, the shape of the droplet is obtained using the shadow image. Theoretically, the shape is governed by the balance of the gravitational and buoyancy forces together with the interfacial tension force acting on the droplet:[63,64]

$$\Delta\rho\, g\, R_{\circ} = \gamma\, B \tag{1}$$

where $\Delta\rho$ is the density difference between the two fluids,[50,65] g is the gravitational acceleration, $R_{\circ}$ is the radius of curvature at the apex of the drop, and B is the shape factor.[66] The shape factor is obtained by solving three dimensionless first-order ordinary differential equations for the coordinates at the surface of the pendant droplet:[64]

$$\frac{dx}{ds} = \cos\cos\phi \tag{2}$$

$$\frac{dz}{ds} = \sin\sin\phi \tag{3}$$

$$\frac{d\phi}{ds} = 2 + B\,z - \frac{\sin\sin\phi}{x} \tag{4}$$

Here, s denotes the contour variable, which varies along the drop surface starting with $s = 0$ at the apex. The above equations are supplemented with the initial conditions at the apex of the drop $x(0) = z(0) = \phi(0) = 0$ (see Figure 1). The drop shape analysis software fits the numerical solution of the above equations to the experimentally captured image and estimates the shape factor B. Finally, γ is calculated via eq 1.

Measurements for multiple droplets were made for a given combination of PB and ionic liquid. Figure 2a,b demonstrates the pendant drop profiles and plot representative values of γ obtained for PB with two ILs, [C_2mim][TFSI], and [C_{10}mim][TFSI], respectively. As the alkyl chain length on the imidazolium ring increases, the γ between PB homopolymer and the ionic liquid decreases as expected. Hence, the ionic liquid with a greater alkyl chain length on its cation progressively becomes less unfavorable to the PB chains. In the context of PB-*b*-PEO micelles, the IL behaves as a progressively less selective solvent for micelle formation as the size of cationic alkyl length increases, which should result in a smaller Q_{eq}.

Micellar Solution Preparation in Mixed ILs. A master solution with a polymer concentration of 1 wt % was prepared by direct dissolution of BO(9−8) in [C_2mim][TFSI] by stirring for 24−48 h at 70 °C. After the micelles are formed, the as-prepared master solution in [C_2mim][TFSI] is then diluted by adding the second ionic liquid, [C_{10}mim][TFSI] at room temperature, such that the polymer

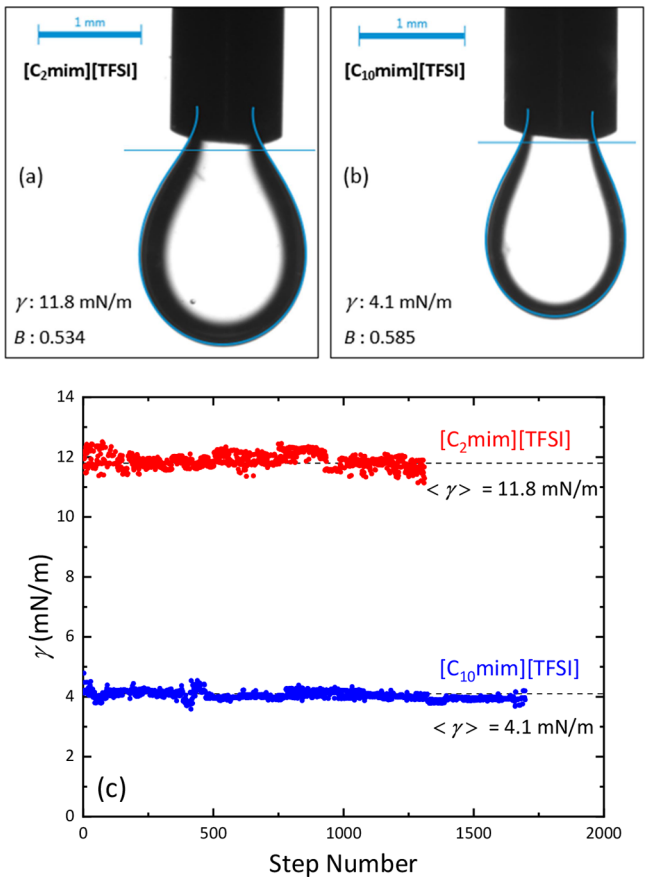

Figure 2. Pendant drop profiles of ionic liquids in the reservoir of PB; (a) [C_2mim][TFSI]; (b) [C_{10}mim][TFSI]. (c) Interfacial tension between 1,2-polybutadiene (PB, M_n = 4.7 kDa) and [C_2mim][TFSI], and [C_{10}mim][TFSI] at 70 °C.

concentration drops below 1 wt %. Depending upon the degree of dilution by the second IL, a series of solutions with concentrations 0.9, 0.8, 0.75. 0.5, 0.25, 0.15, 0.1, and 0.05 wt % of BO(9−8) are obtained. It is important to note that since the dilution is carried out at room temperature, the process and degree of dilution do not greatly influence the size distribution of the as-prepared micelles. Due to lower γ for [C_{10}mim][TFSI] with the core-forming PB block, the dilution amounts to a γ-jump for the as-prepared micelles. After the γ-jump, the micelles were characterized again by DLS, and then the solution was heated and thermally annealed at 170 °C during which the micelles undergo fragmentation. Figure 3 presents a schematic description of the protocol employed to prepare the micellar solution in mixed ILs. Here, IL1 refers to the first ionic liquid in which micelles are prepared, i.e., [C_2mim][TFSI], and IL2 denotes the second ionic liquid used for dilution of the as-prepared micelles to impose the γ-jump, i.e., [C_{10}mim][TFSI]. The micelle size distribution is obtained for the as-prepared micelles (the initial state) as well as for the micelles postfragmentation (the final equilibrium state) using DLS. In addition, in situ DLS measurements have also been carried out during fragmentation to monitor the dynamics of micelle size distribution.

Dynamic Light Scattering (DLS). DLS measurements were carried out to obtain the time variation in average size and size distribution of micelles during fragmentation at 170 °C on a home-built device, including a Brookhaven BI-DS photomultiplier mounted onto an adjustable goniometer, a Lexel Ar^+ laser (wavelength 488 nm), and a Brookhaven BI-9000 correlator. The temperature of the micellar solution is controlled to within ±0.2 °C using an index-matching silicon oil bath. In addition to following micelle size at high temperature during fragmentation, the micelle size and distribution were also obtained at 25 °C using a multiangle DLS instrument fitted with a Brookhaven BI-200SM goniometer coupled with a Brookhaven BI-9000AT correlator

https://doi.org/10.1021/acs.macromol.2c02158
Macromolecules XXXX, XXX, XXX−XXX

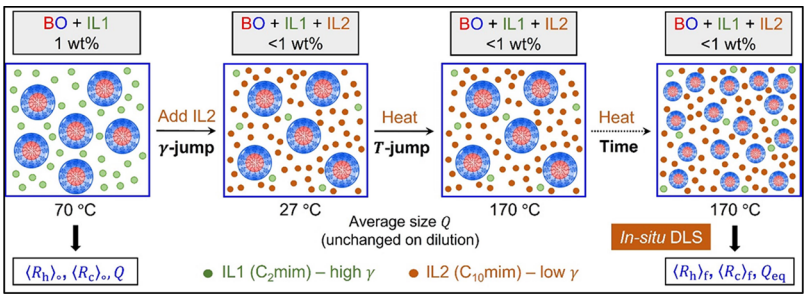

Figure 3. Schematic diagram depicting the protocol to prepare a micellar solution in mixed ILs. The master solution is 1 wt % BO(9−8) in [C_2mim][TFSI] (IL1). The master sample is carefully diluted by adding [C_{10}mim][TFSI] (IL2) at room temperature such that the original micelles remain unaffected. The dilution step is referred to as a γ-jump. Finally, the diluted samples are thermally annealed at 170 °C (referred to as T-jump) to approach an equilibrium state by fragmentation. The kinetics of fragmentation are monitored by in situ DLS measurements.

and 637 nm laser source. DLS samples were prepared by filtering through a 0.45 μm PTFE syringe filters directly into the oven dried dust-free glass tubes with an inner diameter of 0.51 cm. The glass tubes were subsequently flame-sealed under vacuum (60 mTorr) in order to prevent polymer degradation and moisture contamination. While room temperature DLS measurements were carried out at multiple scattering angles from 60° to 120°, the high-temperature in situ DLS measurements were carried out at a fixed scattering angle of 90°.

The normalized measured intensity autocorrelation function $g_2(t)$ was acquired for 1−5 min. The electric field autocorrelation function $g_1(t)$ was obtained from $g_2(t)$ using the Siegert relation[67] $\beta g_1{}^2(t) = g_2(t) - 1$. Fitting the electric field autocorrelation function to a cumulant expansion truncated to second-order, as given below, provides the average decay rate $\bar{\Gamma}$ of the micelles:

$$g_1(t) = A\exp(-\bar{\Gamma}t)\left[1 + \frac{\mu_2}{2\bar{\Gamma}^2}(\bar{\Gamma}t)^2 + \cdots\right] \quad (5)$$

The coefficient of the second-order term provides the variance of the normalized distribution of the decay rates, $\mu_2/\bar{\Gamma}^2$, representing the dispersity of the micelle size distribution. For a reasonably narrow size distribution, the second-order cumulant expansion is sufficient. For any samples exhibiting a bimodal micelle distribution from a regularized positive exponential sum (REPES)[68] analysis and a high dispersity value from the cumulant analysis, the autocorrelation function $g_1(t)$ was fit to a double-exponential function:

$$g_1(t) = A_1\exp(-\bar{\Gamma}_1 t) + A_2\exp(-\bar{\Gamma}_2 t) \quad (6)$$

The apparent average hydrodynamic radius was calculated using the Stokes−Einstein equation

$$\langle R_h\rangle = \frac{k_B T}{6\pi\eta D_t} \quad (7)$$

where k_B is the Boltzmann constant, T is the temperature, $\eta(T)$ is the solvent viscosity, and D_t is the translational diffusion coefficient of the micelles. In the dilute limit, D_t can be approximated by the measured mutual diffusion coefficient, D_m, which was calculated using $D_m = \bar{\Gamma}/q^2$, where q is the magnitude of the scattering vector defined as $q = (4\pi n/\lambda_\circ)\sin(\theta/2)$, $\lambda_\circ$ is the wavelength of light in vacuum, n is the refractive index of the solvent, and θ is the scattering angle. For multiangle measurements, D_m was calculated from a linear fit of $\bar{\Gamma}$ versus q^2 passing through the origin.

Small-Angle X-ray Scattering (SAXS). SAXS measurements were carried out at the Advanced Photon Source, Argonne National Laboratory, on the Sector 5-ID-D beamline of the DuPont-Northwestern-Dow Collaborative Access Team (DND-CAT). SAXS measurements were conducted on micellar solutions corresponding to the initial (before fragmentation) and final (after fragmentation) states at room temperature. The samples were loaded into 1.5 mm diameter borosilicate capillaries and sealed with epoxy under an argon atmosphere. For each capillary, the two-dimensional SAXS data were collected using a Rayonix MX170-HS CCD area detector with an 0.5 s exposure time to X-rays (λ = 0.729 Å), keeping the sample-to-detector distance at 8.5 m. Two-dimensional scattering data were reduced by azimuthal integration to obtain one-dimensional scattering patterns in the form of scattering intensity versus q. The background scattering arising from the surrounding ionic liquid and glass capillary, including an upturn at higher q corresponding to the nanoscale ordering in the solvent,[69] was fit to the power law expression $I(q) = A + Bq^{-m} + Cq^2$, where $2 \le m \le 4$. The background intensity was then subtracted from the solution scattering data. In the case of no upturn at higher q, the background intensity was fit to power law with C set to zero. The background-corrected data were analyzed using the Pederson micelle core-shell model with the Percus−Yevick structure factor.[70,71]

Transmission Electron Microscopy (TEM). An estimate of the average micelle core radius $\langle R_{core}\rangle$ and its standard deviation, σ_{core}, was obtained by performing TEM measurements. Both cryo-TEM and liquid-phase-TEM were conducted on micellar solutions corresponding to the initial (before fragmentation) and final (after fragmentation) states. The imaging was performed using FEI Tecnai G2 Spirit Bio-Twin and Field Emission Gun TEM instruments operating at an accelerating voltage of 120 kV with a 4k × 4k Ultrascan CCD camera with a spot size of 3 or larger. 200 mesh copper grids coated with lacey Formvar stabilized with carbon grids, purchased from Ted Pella Inc., were used for the study. Approximately 0.2 μL of micellar solution was drop-cast on the grid followed by the removal of excess solution using filter paper. While liquid-phase TEM was performed at room temperature, for the cryo-TEM, the sample grids were dipped in liquid nitrogen and were imaged at a temperature of around −190 °C. Each sample was filtered using 0.45 μm PTFE syringe filter to remove any dust prior to grid preparation. For each sample, more than 10 different spots were imaged to capture at least 300 individual micelles. The images were analyzed using ImageJ software.

■ RESULTS AND DISCUSSION

In the following, fragmentation kinetics are studied for the master sample (micelles in a single ionic liquid) as well as the diluted samples (micelles in IL blends). The objective is to examine the effect of the increase in Q/Q_{eq} induced by the jump in γ achieved by dilution. The fragmentation time for the master sample serves as a reference against which the behavior of the diluted samples can be compared in order to uncover the effect of driving force for fragmentation on its kinetics.

Fragmentation Kinetics in a Single Ionic Liquid (IL1). The direct dissolution method typically produces large and somewhat disperse micellar aggregates. In this case, room temperature DLS measurements give the average hydrodynamic radius as $\langle R_h\rangle_\circ \approx 68$ nm with a dispersity of $Đ = 1 + \langle\mu_2/\bar{\Gamma}^2\rangle_\circ \approx 1.27$. The as-prepared micelles are in a kinetically trapped metastable state. Subjecting this master sample to a T-jump followed by thermal annealing at 170 °C provides a strong stimulus, leading to relaxation of micelles toward the equilibrium

https://doi.org/10.1021/acs.macromol.2c02158
Macromolecules XXXX, XXX, XXX−XXX

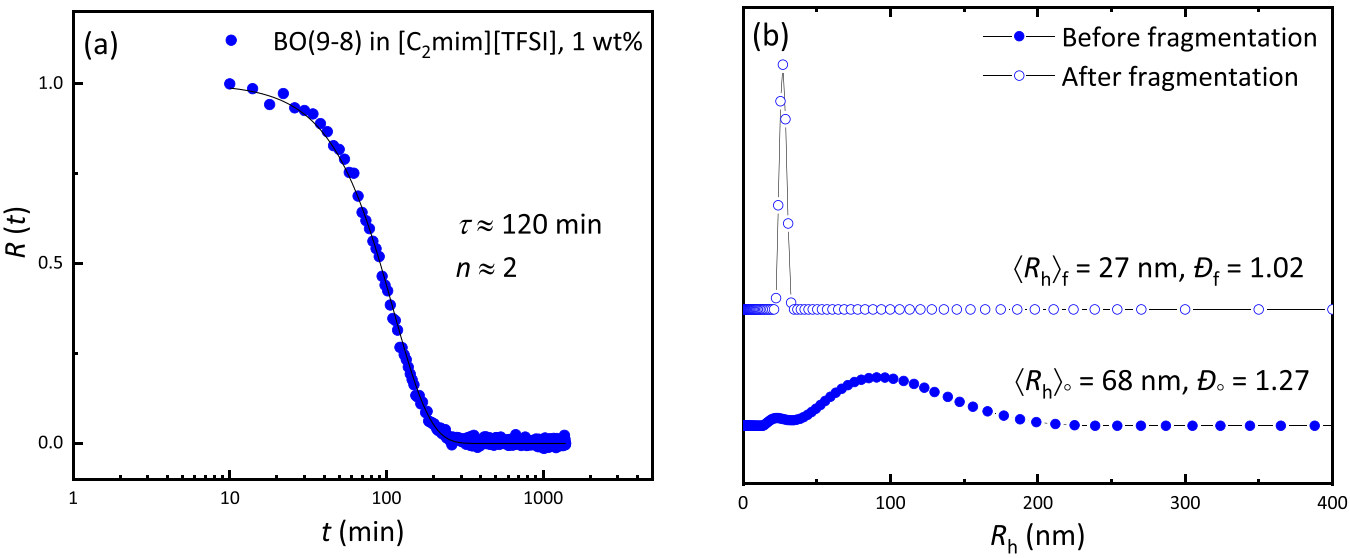

Figure 4. (a) Time variation of the normalized average micelle size for 1 wt % BO(9−8) in pure [C_2mim][TFSI] after T-jump followed by relaxation at 170 °C. Solid line represents the best fit to the Avrami-type equation. (b) Size distribution of as-prepared and steady-state micelles obtained using REPES.

state with a narrower size distribution. The time variation of micelle size given by $\langle R_h(t)\rangle$ is captured using the in situ DLS measurements carried out at 170 °C. The average hydrodynamic radius $\langle R_h(t)\rangle$ is normalized to give the time variation defined as

$$R(t) = \frac{\langle R_h(t)\rangle - \langle R_h(\infty)\rangle}{\langle R_h(0)\rangle - \langle R_h(\infty)\rangle} \tag{8}$$

Here, $\langle R_h(0)\rangle = \langle R_h\rangle_\circ$ and $\langle R_h(\infty)\rangle = \langle R_h\rangle_f$ represent the initial and final average hydrodynamic radii of the micelles, respectively. Figure 4a displays the time decay of the normalized average size of micelles during fragmentation. As in previous reports, the normalized average hydrodynamic radius is found to be well described by the "compressed" exponential function of the form:[49,50]

$$R(t) = \exp\left[-\left(\frac{t}{\tau}\right)^n\right] \tag{9}$$

where τ denotes the characteristic relaxation time for fragmentation and n is the exponent. The as-prepared micelles with $\langle R_h\rangle_\circ \approx 68$ nm fragment to smaller micelles at the steady-state condition (assumed to be near equilibrium) with $\langle R_h\rangle_f \approx 27$ nm. The experimental data for the normalized average radius, $R(t)$, are denoted by symbols in Figure 4a. The experimental size is fit to the compressed exponential described by eq 9 denoted by the solid line with the results $\tau \approx 120$ min and $n \approx 2$. It is important to note that τ is insensitive to the concentration of micelles in a given ionic liquid, as documented previously by Early and Lodge.[50] This is consistent with the predominance of the fragmentation mechanism, which is a first-order process uninfluenced by micelle concentration in the dilute limit. Figure 4b presents the distribution in R_h by REPES before and after fragmentation. The initial broad distribution around the average radius of 68 nm shifts toward a smaller size and attains a nearly monodisperse steady-state condition at the end of the relaxation process (dispersity of 1.02 and average radius of 27 nm).

Fragmentation Kinetics in Mixed ILs. *DLS Measurements.* The 1 wt % master solution of as-prepared micelles of BO(9−8) in [C_2mim][TFSI] (IL1) was diluted by adding various amounts of [C_{10}mim][TFSI] (IL2) such that the as-prepared micelles remain unchanged. Since IL2 exhibits a lower γ with the core-forming PB block compared to IL1, the dilution process amounts to a γ-jump, which modifies the size of the equilibrium micelles. The γ-jump was followed by high-temperature annealing (T-jump) of the diluted solution, and the average micelle size was monitored by in situ DLS. Figure 5

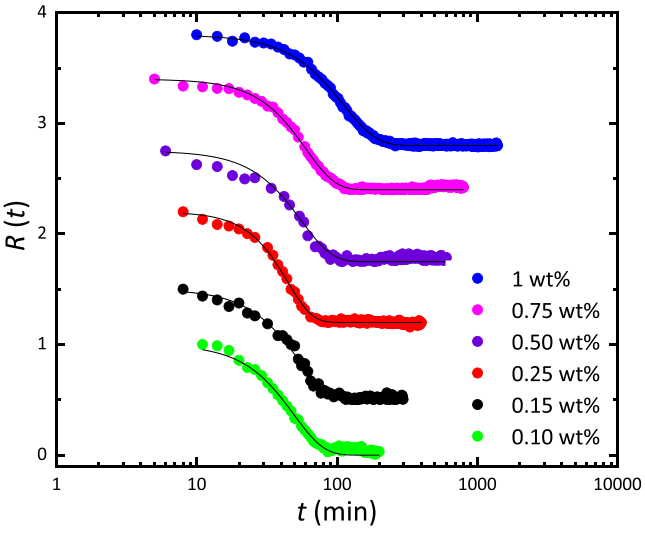

Figure 5. Time dependence of the normalized average hydrodynamic radius $R(t)$ of block copolymer micelles in mixed ILs for various polymer concentrations at a relaxation temperature of 170 °C. Solid lines represent the best fit to the Avrami-type equation. The curves are shifted vertically for clarity.

shows the time-dependence of the normalized average hydrodynamic radius, $R(t)$, for the master solution after dilution to different extents with IL2. The relaxation curves for different concentrations are shifted vertically for clarity. As the degree of dilution increases, the relaxation curve for the average micelle size shifts to the left, indicating faster relaxation kinetics. For all concentrations, $R(t)$ can be described by the compressed-exponential expression given by eq 9. Fitting of the data provides

https://doi.org/10.1021/acs.macromol.2c02158
Macromolecules XXXX, XXX, XXX−XXX

Table 1. Parameters for Micelle Fragmentation from DLS

polymer (P) wt %	(P + IL1):IL2	$\langle R_h \rangle_\circ$ (nm)	$Đ_\circ$	$\langle R_h \rangle_f$ (nm)	$Đ_f$	τ (min)	n
1	1:0	68	1.27	27	1.02	120 ± 20	1.85
0.90	0.90:0.10	70	1.30	27	1.03	66 ± 15	2.01
0.80	0.80:0.20	64	1.31	22	1.04	59 ± 15	2.04
0.75	0.75:0.25	63	1.34	22	1.05	60 ± 15	2.00
0.50	0.50:0.50	67	1.30	26	1.04	56 ± 14	2.01
0.25	0.25:0.75	68	1.24	24	1.01	50 ± 12	1.87
0.15	0.15:0.85	69	1.19	24	1.01	52 ± 12	1.99
0.01	0.10:0.90	67	1.17	23	1.03	49 ± 10	2.00
0.05	0.05:0.95	61	1.17	21	1.03	46 ± 8	1.60

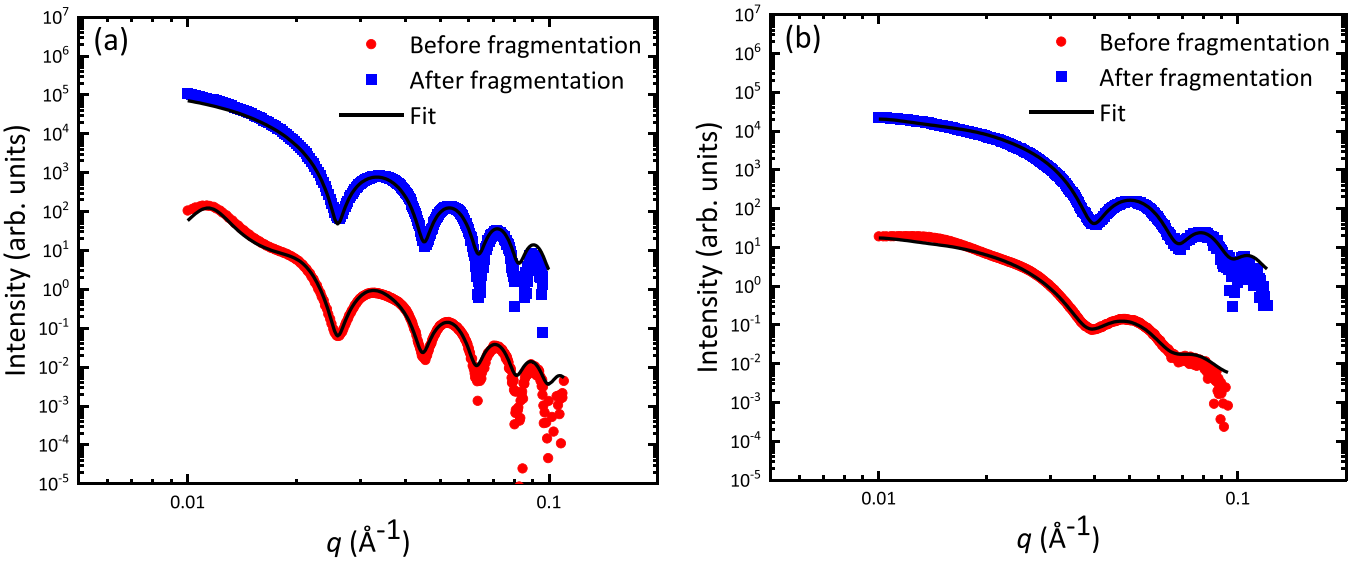

Figure 6. SAXS intensity versus q on logarithmic scales for 1 wt % BO(9−8) in two different single ILs at room temperature: (a) [C_2mim][TFSI] and (b) [C_{10}mim][TFSI]. For each micellar solution, the intensity curves are plotted before and after fragmentation; the final curves are shifted vertically for clarity.

the two kinetic parameters, τ and n; Table 1 summarizes the characteristics of the initial and final micelle size distribution as well as τ and n for varying degrees of dilution.

The protocol adopted for dilution plays an important role. For the γ-jump to be effective, the initial as-prepared micelles should remain intact and unaltered on addition of the second ionic liquid, [C_{10}mim][TFSI], to prepare the diluted solutions. Thus, all the diluted solutions should contain micelles of nearly the same size and initial aggregation number, Q. Indeed, as seen in Table 1, the initial average size of the micelles is essentially independent of concentration in the IL blends. When the diluted solutions are subjected to relaxation after T-jump, the fragmentation process of the as-prepared micelles takes place in solvents of varying compositions and therefore γ. Thus, the size of the final micelles obtained at the end of the relaxation process is expected to be smaller for the more diluted solutions. This is confirmed by the DLS measurements reported in Table 1. The average hydrodynamic radius of the near-equilibrium micelles is found to gradually diminish from 27 to 21 nm as the micellar solution is progressively diluted from 1 to 0.05 wt %. Furthermore, in all cases, the final micelles are much more narrowly distributed in size with $Đ \leq 1.05$.

The characteristic time, τ, is around 120 min for the as-prepared micelles in [C_2mim][TFSI]. Interestingly, as the micellar solution is diluted by addition of [C_{10}mim][TFSI], the fragmentation process accelerates; as concentration decreases from 1 to 0.9 wt%, τ decreases by a factor of two. Upon further diluting the solution from 0.9 to 0.05%, τ decreases more gradually from 66 to 46 min. As the final micelle size becomes smaller, the driving force for fragmentation, represented by the aggregation number ratio Q/Q_{eq}, becomes greater. Thus, faster fragmentation upon dilution can be attributed to enhancement in the driving force. Interestingly, while τ decreases, the exponent n remains ≈ 2 irrespective of the degree of dilution. In summary, a reduction in γ, achieved by addition of lower γ solvent, tends to increase the driving force for fragmentation, which enhances the rate of fragmentation and decreases the final micelle size.

SAXS Measurements. In addition to $\langle R_h \rangle$, it is useful to estimate the average core radius of the micelles $\langle R_{core} \rangle$; the difference provides the average corona thickness of the micelles. The average core radius is also required to estimate the average aggregation number of a micelle, Q. To this end, SAXS measurements were made for micelles before and after relaxation at room temperature. For the master solution of 1 wt % BO(9−8) micelles in [C_2mim][TFSI], Figure 6a shows the scattering intensity $I(q)$ corrected for the background scattering from the solvent in log−log format. The $I(q)$ curves are plotted for micelles before and after the relaxation process; these patterns contain contributions from micelle size, shape, and any intermicellar correlations. The intensity curves for the as-prepared micelles show a small maximum ("structure factor peak") at low q, indicative of the onset of modest interparticle correlation; this maximum disappears after fragmentation. In

https://doi.org/10.1021/acs.macromol.2c02158
Macromolecules XXXX, XXX, XXX−XXX

both cases, form factor oscillations from spherical micellar cores are clearly evident. The q value at the first minimum provides an estimate of the micelle core size as $\langle R\text{core}\rangle \approx 4.493/q\text{min}$. On comparing the SAXS curves for micelles before and after fragmentation, it is evident that the first minimum shifts slightly to higher q, indicative of a decrease in $\langle R_{core}\rangle$ attributed to micelle fragmentation. Similarly, the SAXS patterns for 1 wt % BO(9−8) micelles in pure [C_{10}mim][TFSI] before and after fragmentation are shown in Figure 6b.

To characterize the near-equilibrium micelles resulting from fragmentation, SAXS measurements were also carried out for the diluted solutions after fragmentation. Figure 7 displays the SAXS

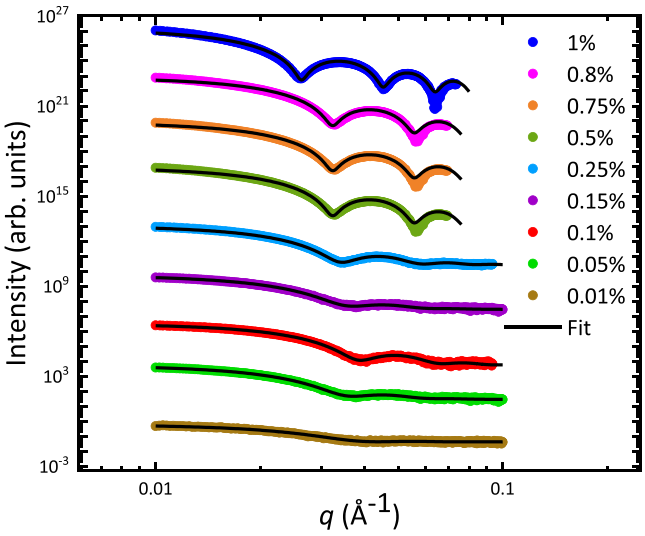

Figure 7. SAXS intensity versus q on logarithmic scales for BO(9−8) at different degrees of dilution in mixed ILs. The intensity curves are plotted for the solution of micelles at the steady-state (i.e., equilibrium state attained after fragmentation). The curve for concentration of 1% represents the master solution, and the rest of the curves represent the diluted samples by adding second ionic liquid. The curves are shifted vertically by a factor of 10^3 for clarity. Measurements were acquired at room temperature after quenching each sample in a water bath. Solid lines represent fit using core-shell model.

intensity curves, corrected for background intensity, for solutions with varying degrees of dilution. As the degree of dilution increases, the first minimum shifts toward higher q, indicating smaller average micelle cores. The reduction in equilibrium micelle size with dilution is attributed to the decrease in γ by addition of the second ionic liquid. In addition to shifting the first minimum, the general character of $I(q)$ is also altered by dilution. In particular, the multiple distinguishable minima, clearly identifiable for relatively high concentrations, are suppressed and eventually eliminated by dilution. This could be the result of significantly lower signal-to-noise or a broadening of the final micelle core size distribution; the DLS results in Table 1 suggest the former is the dominant effect.

The micelle characteristics estimated from SAXS measurements are summarized in Table 2. The micelle core radius $\langle R_{core}\rangle_f$ is estimated by fitting the SAXS intensity curves. The aggregation number of the final micelles, Q_{eq}, is calculated using $\langle R_{core}\rangle_f$, assuming no solvent in the core. Q/Q_{eq}, the ratio of aggregation numbers of initial (as-prepared) and final (equilibrium) micelles, represents the measure of driving force for fragmentation. Micelles in a surrounding medium of progressively lower γ are found to have relatively smaller core

Table 2. Micelle Characteristics after Fragmentation from SAXS

polymer (P) (wt %)	(P + IL1):IL2	$\langle R_{core}\rangle_f$ (nm)	σ_{core} (nm)	Q_{eq}	Q/Q_{eq}
1	1:0	17.1	0.5	1280	1.1
0.90	0.90:0.10	16.4	0.6	1130	1.2
0.80	0.80:0.20	14	0.5	700	2
0.75	0.75:0.25	14	0.6	700	2
0.50	0.50:0.50	13.2	0.8	600	2.3
0.25	0.25:0.75	13.2	0.8	585	2.3
0.15	0.15:0.85	12.5	1.2	500	2.7
0.10	0.10:0.90	11.8	0.9	420	3.2
0.05	0.05:0.95	11	0.7	340	4
0.01	0.01:0.99	10.5	0.8	295	4.6

sizes at equilibrium. This reduction in $\langle R_{core}\rangle$ implies a lower aggregation number, Q_{eq}. As seen in Table 2, Q_{eq} decreases from around 1280 for the 1 wt % solution in IL1 to around 270 for the 0.01 wt % micellar solution. The reduction in Q_{eq} with lowing γ is found to follow a power-law relation $Q_{eq} \sim \gamma^{6/5}$ as shown in Figure S11. The experimentally obtained dependence of Q_{eq} on γ is broadly consistent with the scaling predictions.[30] It is important to note that for all the diluted samples, the average micelle size before fragmentation remains the same, corresponding to the as-prepared micelles. The average aggregation number before fragmentation, determined from the SAXS pattern in Figure 6a, is $Q \approx 1350$. A reduction in Q_{eq} by dilution, therefore, implies enhancement in the driving force for fragmentation.

Transmission Electron Microscopy. To gain further insight on micelle core size and shape, cryo-TEM was performed on micelle solutions before and after fragmentation. For the master solution, Figure 8a,b presents electron micrographs before and after thermal annealing, respectively. The electron density contrast between PB (core-forming chains with lower electron density) and PEO-plus-ionic liquid (corona-forming chains and solvent with higher electron density) enables the micelle cores to appear as distinct bright regions embedded in a dark matrix. The

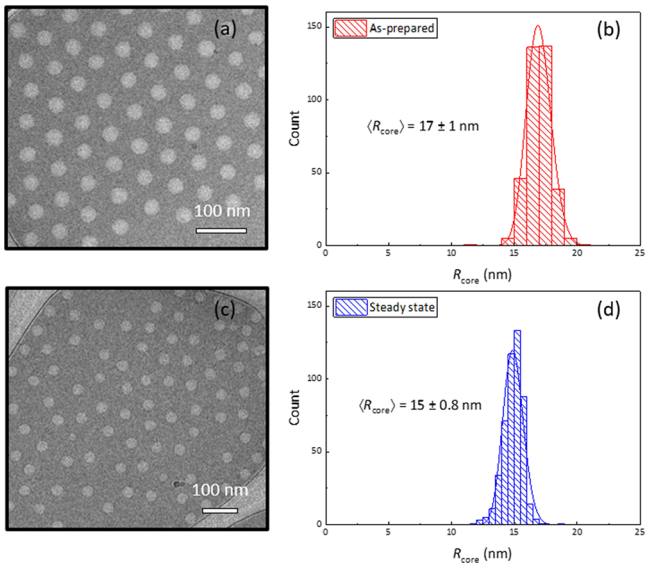

Figure 8. Cryo-TEM micrographs and the corresponding histograms of 1 wt % BO(9−8) in [C_2mim][TFSI] (master solution). Bright spots indicate micelle core (PB chains). (a,b) As-prepared micelles (before fragmentation); (c,d) after thermal annealing (after fragmentation).

https://doi.org/10.1021/acs.macromol.2c02158
Macromolecules XXXX, XXX, XXX−XXX

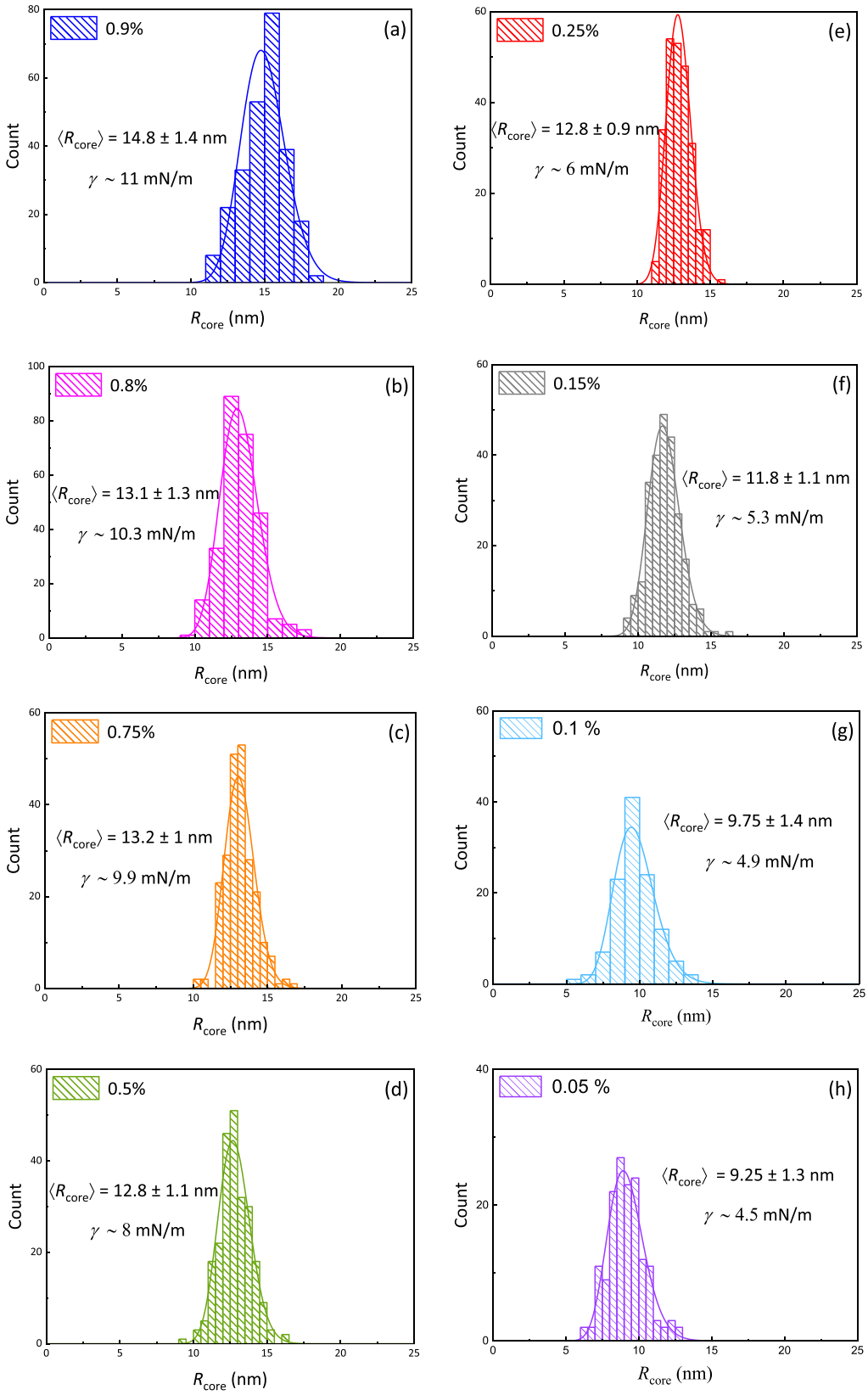

Figure 9. Histograms corresponding to the TEM images presented in Figure S9 for distribution of core diameter of BO(9−8) micelles after fragmentation in mixed ILs at different polymer concentration. (a) 0.9%; (b) 0.8%; (c) 0.75%; (d) 0.5%; (e) 0.25%; (f) 0.15%; (g) 0.1%; and (h) 0.05%.

micrographs clearly show that the micelle cores are spherical in shape. Image analysis yielded histograms of micelle core size, using ca. 200−600 micelles for each solution, with the bin size set to 2 nm. The discrete distributions were fit to a lognormal

https://doi.org/10.1021/acs.macromol.2c02158
Macromolecules XXXX, XXX, XXX−XXX

distribution, indicated by the solid lines in the figure. The average micelle core diameter $\langle R_{core} \rangle$ and standard deviation σ_{core} are noted in the histograms. The as-prepared BO(9−8) micelles in pure [C_2mim][TFSI] have $\langle R_{core} \rangle$ of 17 ± 1 nm. After fragmentation, the $\langle R_{core} \rangle$ decreases to 15 ± 0.8 nm, while the spherical shape persists. SAXS measurements estimated the $\langle R_{core} \rangle$ of as-prepared micelles to be 17.4 nm. Thus, the average core size estimates from the TEM analysis are in close agreement with those obtained from the SAXS.

TEM analysis was also conducted on the diluted micellar solutions after fragmentation. Figure 9a−h presents histograms for the diluted solutions at steady-state; the corresponding electron micrographs are provided in the Supporting Information, Figure S9. The drop in polymer concentration from 1 to 0.1 wt % yields a decreasing γ, which results in smaller micelles at equilibrium as clearly depicted in Figure 9a−h; overall $\langle R_{core} \rangle$ decreases from around 15 to 9 nm. As can also be seen from the micrographs (Figure S9), the contrast apparently becomes weaker due to the changing electron density in the blended ILs.

The micelle core sizes obtained from TEM are generally in good agreement with those obtained from SAXS. As with SAXS measurements, the average core radius can be used to calculate Q as listed in Table 3. As noted earlier, for any diluted sample, the aggregation number of the initial as-prepared micelles, Q, remains the same and the aggregation number for micelles postfragmentation, Q_{eq}, decreases as the extent of dilution increases. Thus, the size ratio Q/Q_{eq} increases over a broad range from 1.5 to around 6.2.

Table 3. Micelle Characteristics after Fragmentation from Cryo-TEM

polymer (P) (wt %)	(P + IL1):IL2	$\langle R_{core} \rangle_f$ (nm)	σ_{core} (nm)	Q_{eq}	Q/Q_{eq}
1	1:0	15	0.8	861	1.5
0.90	0.90:0.10	14.8	1.4	827	1.5
0.80	0.80:0.20	13.1	1.3	573	2.2
0.75	0.75:0.25	13.2	1	580	2.2
0.50	0.50:0.50	12.8	1.1	535	2.3
0.25	0.25:0.75	12.8	0.9	535	2.3
0.15	0.15:0.85	11.8	1.1	419	3
0.10	0.10:0.90	9.75	1.4	236	5.3
0.05	0.05:0.95	9.25	1.3	202	6.2

It is important to note that the transformation from larger to smaller spherical micelles increases the interfacial area per chain. Hence, the process is not driven by a change in interfacial tension; nor is it related to the Rayleigh instability. Rather, relief of chain stretching is likely the mechanism responsible for fragmentation.[51,61] The change in solvent changes the distance to equilibrium but not the direction. Even in the case of no change in solvent quality, micelles still relax by fragmentation as shown in Figure 4a. It should also be noted that the initial as-prepared micelles are not unstable, but actually deeply metastable, with a barrier exceeding 20 kT.[49,50]

Effect of Thermodynamic Driving Force on Fragmentation Kinetics. The direct dissolution method generates block copolymer micelles that are significantly larger than the equilibrium size, i.e., $Q/Qeq > 1$. The relaxation of as-prepared micelles to approach equilibrium under a T-jump is dominated by micelle fragmentation under the conditions of the present study. The size ratio of micelles before and after relaxation, Q/Q_{eq}, can be treated as the measure of driving force for the fragmentation process. In prior studies, the micelles were prepared and then allowed to relax under a T-jump in the same solvent. The solvent quality represented by its interfacial tension with the core-forming block influences the equilibrium size of the micelles as micelle size is directly related to γ. When micelles are prepared and fragmented in the same solvent, either pure or mixed ILs, the value of γ influences both Q and Q_{eq} in the same way. Thus, irrespective of the nature of solvent quality, the ratio Q/Q_{eq} remains nearly unaffected.[50] The protocol adopted in prior studies, therefore, does not allow one to isolate the role of the driving force for fragmentation in its kinetics. In the present protocol, dilution of the master solution with the second ionic liquid enables control of the size ratio Q/Q_{eq} over a broad range.

Figure 10a depicts the effect of Q/Q_{eq} on the relaxation time τ. The increase in driving force results in significantly faster fragmentation kinetics. The decrease in relaxation time is much sharper for $Q/Qeq \approx 1.2 - 5$, and particularly for $Q/Q_{eq} \leq 2$. For $Q/Qeq > 5$, the characteristic relaxation time approaches a plateau value, corresponding to the relaxation time for micelle equilibration in pure [C_{10}mim][TFSI] (IL2). Faster fragmentation of bigger micelles can be explained with the help of micelle free energy. For $Q/Q_{eq} > 2$, the as-prepared micelles are much

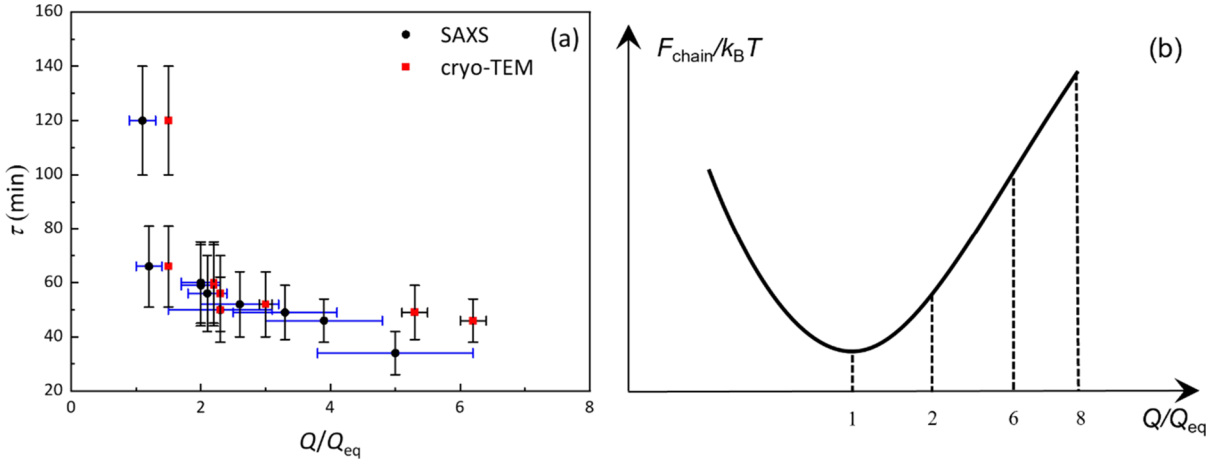

Figure 10. (a) Variation of fragmentation time, τ, with the micelle size ratio Q/Q_{eq} based on SAXS and cryo-TEM results. The error bars represent the standard error from the fits in τ and in Q (propagated from R_{core}). (b) Schematic free energy plot.

https://doi.org/10.1021/acs.macromol.2c02158
Macromolecules XXXX, XXX, XXX−XXX

bigger than the equilibrium size and experience significant crowding of corona chains leading to higher free energy associated with corona stretching. The conformational energy cost dominates the interfacial energy associated with the creation of smaller micelles and provides the thermodynamic driving force for fragmentation. As Q/Q_{eq} increases, the thermodynamic driving force increases, resulting in faster fragmentation even though the initial micelles are farther away from the equilibrium size. Quite possibly these micelles undergo a cascade of fragmentation events, which are progressively slower as Q/Q_{eq} approaches 2 from above. Alternatively, these micelles could undergo spontaneous fragmentation into multiple "daughter micelles," essentially simultaneously. In order to distinguish these two possibilities, in situ time-resolved TEM measurements are needed.

A qualitative free energy landscape for micelles in the neighborhood of $Q/Q_{eq} > 1$ is shown in Figure 10b. For micelles with $Q/Q_{eq} \geq 1.2-2$, fragmentation is energetically favorable as it produces smaller micelles with collective energy smaller than the initial state. For micelles with $Q/Q_{eq} \leq 2$, the fragmentation is relatively less favorable as it produces some micelles below the equilibrium size with higher total energy than the equilibrium micelle. In this size range, the process of fragmentation is not necessarily a net downhill process and should therefore slow down considerably.

■ SUMMARY

The kinetics of fragmentation in block copolymer micelles was investigated to explore the role of the thermodynamic driving force. Spherical micelles of PB-*b*-PEO were prepared by direct dissolution in an ionic liquid. Relaxation of the as-prepared micelles (aggregation number $Q > Q_{eq}$) to attain an equilibrium state (aggregation number $\approx Q_{eq}$) predominantly through fragmentation was studied. Importantly, we varied the driving force for fragmentation, represented by Q/Q_{eq}, by strategic mixing of different ILs as solvents. The choice of a pair of ILs to be used for mixing was made based on the measured γ of the solvent with the micelle core, which was determined using a pendant drop technique. The micelles prepared in a given solvent ([C_2mim][TFSI]) were subjected to fragmentation in a series of surrounding media of progressively lower selectivity. Altering the solvent quality was accomplished by addition of the second solvent ([C_{10}mim][TFSI]) with a lower γ with the core-forming PB block compared to the first solvent. The reduction in γ of the solvent mixture leads to the formation of smaller micelles postfragmentation. By controlling the amount of low γ solvent being added to the micellar solution, the size ratio Q/Q_{eq} varied from 1.2 to 5.

The average micelle size during the equilibration process obtained using in situ DLS at 170 °C was described using a compressed exponential expression, and the characteristic fragmentation time was obtained. SAXS and TEM were used to quantify the average core size before and after fragmentation with consistent results. Assuming "dry" micellar cores, these measurements gave access to the aggregation numbers of the micelles. As the size difference between the as-prepared and equilibrium micelles became wider (indicated by higher values for the ratio Q/Q_{eq}), the fragmentation time was found to decrease. Thus, an increase in the driving force for fragmentation tends to systematically enhance the rate of fragmentation. The faster fragmentation of larger micelles can be understood in terms of increasingly crowded corona chains. It is not yet possible to distinguish whether larger micelles undergo a cascade of fragmentation events to achieve Q_{eq} or whether larger micelles fragment into more than two "daughter" micelles.

■ ASSOCIATED CONTENT

Supporting Information

The Supporting Information is available free of charge at https://pubs.acs.org/doi/10.1021/acs.macromol.2c02158.

^{1}H NMR spectra of BO(9−8), [C_2mim][TFSI], and [C_{10}mim][TFSI], SEC-RI traces of PB(5 k), and BO(9−8) in THF, SAXS profile of BO(9−8) in bulk, SAXS patterns of pure [C_2mim][TFSI] and [C_{10}mim][TFSI] and their mixtures, REPES results of BO(9−8) in mixed ILs, cryo-TEM micrographs of BO(9−8) micelles after fragmentation at different degrees of dilution in mixed ILs, room temperature LP-TEM micrographs of BO(9−8) in [C_2mim][TFSI], Q_{eq} vs γ for BO(9−8) in mixed ILs, ionic liquid parameters, and core-shell contrast values (PDF)

■ AUTHOR INFORMATION

Corresponding Author

Timothy P. Lodge − *Department of Chemistry and Department of Chemical Engineering and Materials Science, University of Minnesota, Minneapolis, Minnesota 55455-0431, United States;* orcid.org/0000-0001-5916-8834; Email: lodge@umn.edu

Author

Supriya Gupta − *Department of Chemistry, University of Minnesota, Minneapolis, Minnesota 55455-0431, United States;* orcid.org/0000-0002-0105-3855

Complete contact information is available at: https://pubs.acs.org/10.1021/acs.macromol.2c02158

Notes

The authors declare no competing financial interest.

■ ACKNOWLEDGMENTS

This work was financially supported by the National Science Foundation Polymers Program through Award DMR-2103630. Dr. Julia Early provided the polymer used in the study. SAXS experiments were performed at the 5-ID-D beamline of the DND-CAT at the Advanced Photon Source, Argonne National Laboratory. The authors acknowledge Prof. Lorraine Francis for providing access to the KRÜSS DSA-30S tensiometer for the measurement of γ, and Prof. Lynn Walker for helpful discussions. Part of this work was carried out in the Characterization Facility, College of Science and Engineering, University of Minnesota, which receives partial support from the NSF through the MRSEC (Award no. DMR-2011401) and the NNCI (Award no. ECCS-2025124) programs. We also thank Dr. Wei Zhang for help with the TEM imaging.

■ REFERENCES

(1) Bates, C. M.; Bates, F. S. *50th Anniversary Perspective*: Block Polymers—Pure Potential. *Macromolecules* **2017**, *50*, 3−22.

(2) Gohy, J. F. Block Copolymer Micelles. *Adv. Polym. Sci.* **2005**, *190*, 65−136.

(3) Mai, Y.; Eisenberg, A. Self-Assembly of Block Copolymers. *Chem. Soc. Rev.* **2012**, *41*, 5969−5985.

(4) Tritschler, U.; Pearce, S.; Gwyther, J.; Whittell, G. R.; Manners, I. *50th Anniversary Perspective*: Functional Nanoparticles from the

Solution Self-Assembly of Block Copolymers. *Macromolecules* **2017**, *50*, 3439−3463.
(5) Bates, F. S.; Fredrickson, G. H. Block Copolymers—Designer Soft Materials. *Phys. Today* **2000**, *52*, 32.
(6) Leibler, L. Theory of Microphase Separation in Block Copolymers. *Macromolecules* **1980**, *13*, 1602−1617.
(7) Matsen, M. W.; Schick, M. Stable and Unstable Phases of a Diblock Copolymer Melt. *Phys. Rev. Lett.* **1994**, *72*, 2660−2663.
(8) Fredrickson, G. H. *The Equilibrium Theory of Inhomogeneous Polymers*; Oxford University Press, 2013.
(9) Noolandi, J.; Hong, K. M. Theory of Block Copolymer Micelles in Solution. *Macromolecules* **1983**, *16*, 1443−1448.
(10) Gupta, S.; Chokshi, P. Self-Organization of a 4-Miktoarm Star Block Copolymer Induced by Cylindrical Confinement. *Soft Matter* **2021**, *17*, 4929−4941.
(11) Ge, Z.; Liu, S. Functional Block Copolymer Assemblies Responsive to Tumor and Intracellular Microenvironments for Site-Specific Drug Delivery and Enhanced Imaging Performance. *Chem. Soc. Rev.* **2013**, *42*, 7289−7325.
(12) Hubbell, J. A. Enhancing Drug Function. *Science* **2003**, *300*, 595−596.
(13) Elsabahy, M.; Heo, G. S.; Lim, S. M.; Sun, G.; Wooley, K. L. Polymeric Nanostructures for Imaging and Therapy. *Chem. Rev.* **2015**, *115*, 10967−11011.
(14) Monteiro, M. Nanoreactors for Polymerizations and Organic Reactions. *Macromolecules* **2010**, *43*, 1159−1168.
(15) Krishnamoorthy, S.; Pugin, R.; Brugger, J.; Heinzelmann, H.; Hinderling, C. Nanopatterned Self-Assembled Monolayers by Using Diblock Copolymer Micelles as Nanometer-Scale Adsorption and Etch Masks. *Adv. Mater.* **2008**, *20*, 1962−1965.
(16) Wang, T. Y.; Tsiang, R. C. C.; Liou, J. S.; Wu, J.; Sheu, H. C. Preparation and Characterization of a Star-Shaped Polystyrene-*b*-Poly(Ethylene-*co*-Propylene) Block Copolymer as a Viscosity Index Improver of Lubricant. *J. Appl. Polym. Sci.* **2001**, *79*, 1838−1846.
(17) Halperin, A. Polymeric Micelles: A Star Model. *Macromolecules* **1987**, *20*, 2943−2946.
(18) Halperin, A.; Tirrell, M.; Lodge, T. P. Tethered Chains in Polymer Microstructures. *Adv. Polym. Sci.* **1992**, *100*, 31−71.
(19) Nagarajan, R.; Ganesh, K. Block Copolymer Self-Assembly in Selective Solvents: Spherical Micelles with Segregated Cores. *J. Chem. Phys.* **1989**, *90*, 5843−5856.
(20) Pépin, M. P.; Whitmore, M. D. Monte Carlo and Mean Field Study of Diblock Copolymer Micelles. *Macromolecules* **2000**, *33*, 8644−8653.
(21) Zhulina, E. B.; Adam, M.; LaRue, I.; Sheiko, S. S.; Rubinstein, M. Diblock Copolymer Micelles in a Dilute Solution. *Macromolecules* **2005**, *38*, 5330−5351.
(22) He, Y.; Li, Z.; Simone, P.; Lodge, T. P. Self-Assembly of Block Copolymer Micelles in an Ionic Liquid. *J. Am. Chem. Soc.* **2006**, *128*, 2745−2750.
(23) Denkova, A. G.; Mendes, E.; Coppens, M. O. Non-Equilibrium Dynamics of Block Copolymer Micelles in Solution: Recent Insights and Open Questions. *Soft Matter* **2010**, *6*, 2351−2357.
(24) Zana, R. Dynamics in Micellar Solutions of Amphiphilic Block Copolymers. In *Dynamics of Surfactant Self-Assemblies: Micelles, Microemulsions, Vesicles, and Lyotropic Phases*; Hubbard, A. T., Ed.; Taylor & Francis Group/CRC Press: Boca Raton, 2005; pp 161−231.
(25) Aniansson, E. A. G.; Wall, S. N. Kinetics of Step-Wise Micelle Association. *J. Phys. Chem.* **1974**, *78*, 1024−1030.
(26) Aniansson, E. A. G.; Wall, S. N. Kinetics of Step-Wise Micelle Association. Correction and Improvement. *J. Phys. Chem.* **1975**, *79*, 857−858.
(27) Aniansson, E. A. G.; Wall, S. N.; Almgren, M.; Hoffmann, H.; Kielmann, I.; Ulbricht, W.; Zana, R.; Lang, J.; Tondre, C. Theory of the Kinetics of Micellar Equilibria, and Quantitative Interpretation of Chemical Relaxation Studies of Micellar Solutions of Ionic Surfactants. *J. Phys. Chem.* **1976**, *80*, 905−922.
(28) Halperin, A.; Alexander, S. Polymeric Micelles: Their Relaxation Kinetics. *Macromolecules* **1989**, *22*, 2403−2412.
(29) Halperin, A. On Micellar Exchange: The Role of the Insertion Penalty. *Macromolecules* **2011**, *44*, 5072−5074.
(30) Dormidontova, E. E. Micellization Kinetics in Block Copolymer Solutions: Scaling Model. *Macromolecules* **1999**, *32*, 7630−7644.
(31) Wang, Y.; Balaji, R.; Quirk, R. P.; Mattice, W. L. Detection of the Rate of Exchange of Chains between Micelles Formed by Diblock Copolymers in Aqueous Solution. *Polym. Bull.* **1992**, *28*, 333−338.
(32) Cao, T.; Munk, P.; Ramireddy, C.; Tuzar, Z.; Webber, S. E. Fluorescence Studies of Amphiphilic Poly(Methacrylic Acid)-Block-Polystyrene-Block-Poly(Methacrylic Acid) Micelles. *Macromolecules* **1991**, *24*, 6300−6305.
(33) Smith, C. K.; Liu, G. Determination of the Rate Constant for Chain Insertion into Poly(Methyl Methacrylate)-*Block*-Poly-(Methacrylic Acid) Micelles by a Fluorescence Method. *Macromolecules* **1996**, *29*, 2060−2067.
(34) Willner, L.; Poppe, A.; Allgaier, J.; Monkenbusch, M.; Richter, D. Time-Resolved SANS for the Determination of Unimer Exchange Kinetics in Block Copolymer Micelles. *Europhys. Lett.* **2001**, *55*, 667−673.
(35) Won, Y.-Y.; Davis, H. T.; Bates, F. S. Molecular Exchange in PEO−PB Micelles in Water. *Macromolecules* **2003**, *36*, 953−955.
(36) van Stam, J.; Creutz, S.; De Schryver, F. C.; Jérôme, R. Tuning of the Exchange Dynamics of Unimers between Block Copolymer Micelles with Temperature, Cosolvents, and Cosurfactants. *Macromolecules* **2000**, *33*, 6388−6395.
(37) Lu, J.; Bates, F. S.; Lodge, T. P. Remarkable Effect of Molecular Architecture on Chain Exchange in Triblock Copolymer Micelles. *Macromolecules* **2015**, *48*, 2667−2676.
(38) Choi, S.; Lodge, T. P.; Bates, F. S. Mechanism of Molecular Exchange in Diblock Copolymer Micelles: Hypersensitivity to Core Chain Length. *Phys. Rev. Lett.* **2010**, *104*, No. 047802.
(39) Zhao, D.; Ma, Y.; Lodge, T. P. Exchange Kinetics for a Single Block Copolymer in Micelles of Two Different Sizes. *Macromolecules* **2018**, *51*, 2312−2320.
(40) Ma, Y.; Lodge, T. P. Chain Exchange Kinetics in Diblock Copolymer Micelles in Ionic Liquids: The Role of χ. *Macromolecules* **2016**, *49*, 9542−9552.
(41) Seeger, S. C.; Dorfman, K. D.; Lodge, T. P. Free Energy Trajectory for Escape of a Single Chain from a Diblock Copolymer Micelle. *ACS Macro Lett.* **2021**, *10*, 1570−1575.
(42) Rharbi, Y. Fusion and Fragmentation Dynamics at Equilibrium in Triblock Copolymer Micelles. *Macromolecules* **2012**, *45*, 9823−9826.
(43) Landazuri, G.; Fernandez, V. V. A.; Soltero, J. F. A.; Rharbi, Y. Length of the Core Forming Block Effect on Fusion and Fission Dynamics at Equilibrium in PEO−PPO−PEO Triblock Copolymer Micelles in the Spherical Regime. *Macromolecules* **2021**, *54*, 2494−2505.
(44) Lodge, T. P.; Seitzinger, C. L.; Seeger, S. C.; Yang, S.; Gupta, S.; Dorfman, K. D. Dynamics and Equilibration Mechanisms in Block Copolymer Particles. *ACS Polym. Au* **2022**, 397.
(45) Zhang, L.; Eisenberg, A. Thermodynamic vs Kinetic Aspects in the Formation and Morphological Transitions of Crew-Cut Aggregates Produced by Self-Assembly of Polystyrene-*b*-Poly(Acrylic Acid) Block Copolymers in Dilute Solution. *Macromolecules* **1999**, *32*, 2239−2249.
(46) Desbaumes, L.; Eisenberg, A. Single-Solvent Preparation of Crew-Cut Aggregates of Various Morphologies from an Amphiphilic Diblock Copolymer. *Langmuir* **1999**, *15*, 36−38.
(47) Cameron, N. S.; Corbierre, M. K.; Eisenberg, A. *1998 E.W.R. Steacie Award Lecture*: Asymmetric Amphiphilic Block Copolymers in Solution: A Morphological Wonderland. *Can. J. Chem.* **1999**, *77*, 1311−1326.
(48) Meli, L.; Lodge, T. P. Equilibrium vs Metastability: High-Temperature Annealing of Spherical Block Copolymer Micelles in an Ionic Liquid. *Macromolecules* **2009**, *42*, 580−583.
(49) Meli, L.; Santiago, J. M.; Lodge, T. P. Path-Dependent Morphology and Relaxation Kinetics of Highly Amphiphilic Diblock Copolymer Micelles in Ionic Liquids. *Macromolecules* **2010**, *43*, 2018−2027.

https://doi.org/10.1021/acs.macromol.2c02158
Macromolecules XXXX, XXX, XXX−XXX

(50) Early, J. T.; Lodge, T. P. Fragmentation of 1,2-Polybutadiene-Block-Poly(Ethylene Oxide) Micelles in Imidazolium-Based Ionic Liquids. *Macromolecules* **2019**, *52*, 7089−7101.
(51) Early, J. T.; Block, A.; Yager, K. G.; Lodge, T. P. Molecular Weight Dependence of Block Copolymer Micelle Fragmentation Kinetics. *J. Am. Chem. Soc.* **2021**, *143*, 7748−7758.
(52) Wang, E.; Zhu, J.; Zhao, D.; Xie, S.; Bates, F. S.; Lodge, T. P. Effect of Solvent Selectivity on Chain Exchange Kinetics in Block Copolymer Micelles. *Macromolecules* **2019**, *53*, 417−426.
(53) Zhao, D.; Wang, E.; Lodge, T. P. Hybridization of a Bimodal Distribution of Copolymer Micelles. *Macromolecules* **2020**, *53*, 7705−7716.
(54) Lund, R.; Willner, L.; Stellbrink, J.; Radulescu, A.; Richter, D. Role of Interfacial Tension for the Structure of PEP−PEO Polymeric Micelles. A Combined SANS and Pendant Drop Tensiometry Investigation. *Macromolecules* **2004**, *37*, 9984−9993.
(55) Wang, E.; Lu, J.; Bates, F. S.; Lodge, T. P. Effect of Corona Block Length on the Structure and Chain Exchange Kinetics of Block Copolymer Micelles. *Macromolecules* **2018**, *51*, 3563−3571.
(56) Lund, R.; Willner, L.; Richter, D.; Dormidontova, E. E. Equilibrium Chain Exchange Kinetics of Diblock Copolymer Micelles: Tuning and Logarithmic Relaxation. *Macromolecules* **2006**, *39*, 4566−4575.
(57) Lund, R.; Willner, L.; Richter, D.; Lindner, P.; Narayanan, T. Kinetic Pathway of the Cylinder-to-Sphere Transition in Block Copolymer Micelles Observed in Situ by Time-Resolved Neutron and Synchrotron Scattering. *ACS Macro Lett.* **2013**, *2*, 1082−1087.
(58) Wang, L.; Huang, H.; He, T. Rayleigh Instability Induced Cylinder-to-Sphere Transition in Block Copolymer Micelles: Direct Visualization of the Kinetic Pathway. *ACS Macro Lett.* **2014**, *3*, 433−438.
(59) Zhou, Y.; Yan, D. Real-Time Membrane Fusion of Giant Polymer Vesicles. *J. Am. Chem. Soc.* **2005**, *127*, 10468−10469.
(60) Parent, L. R.; Bakalis, E.; Ramírez-Hernández, A.; Kammeyer, J. K.; Park, C.; de Pablo, J.; Zerbetto, F.; Patterson, J. P.; Gianneschi, N. C. Directly Observing Micelle Fusion and Growth in Solution by Liquid-Cell Transmission Electron Microscopy. *J. Am. Chem. Soc.* **2017**, *139*, 17140−17151.
(61) Early, J. T.; Yager, K. G.; Lodge, T. P. Direct Observation of Micelle Fragmentation via In Situ Liquid-Phase Transmission Electron Microscopy. *ACS Macro Lett.* **2020**, *9*, 756−761.
(62) Gao, J.; Li, S.; Zhang, X.; Wang, W. Computer Simulations of Micelle Fission. *Phys. Chem. Chem. Phys.* **2010**, *12*, 3219−3228.
(63) Bashforth, F.; Adams, J. C. *An Attempt to Test the Theories of Capillary Action by Comparing the Theoretical and Measured Forms of Drops of Fluid*; University Press, 1883.
(64) Berry, J. D.; Neeson, M. J.; Dagastine, R. R.; Chan, D. Y.; Tabor, R. F. Measurement of Surface and Interfacial Tension using Pendant Drop Tensiometry. *J. Colloid Interface Sci.* **2015**, *454*, 226−237.
(65) Tariq, M.; Serro, A. P.; Mata, J. L.; Saramago, B.; Esperança, J. M.; Lopes, J. N. C.; Rebelo, L. P. N. High-Temperature Surface Tension and Density Measurements of 1-Alkyl-3-Methylimidazolium Bistriflamide Ionic Liquids. *Fluid Phase Equilib.* **2010**, *294*, 131−138.
(66) Bond, W.; Newton, D. A. Bubbles, Drops, and Stokes' Law. *London, Edinburgh Dublin Philos. Mag. J. Sci.* **1928**, *5*, 794−800.
(67) Brown, W. *Dynamic Light Scattering: The Method and Some Applications (Monographs on the Physics and Chemistry of Materials; 49)*; Clarendon Press; Oxford University Press: Oxford (England); New York, 1993.
(68) Jakeš, J. Testing of the Constrained Regularization Method of Inverting Laplace Transform on Simulated Very Wide Quasielastic Light Scattering Autocorrelation Functions. *Czech. J. Phys.* **1988**, *38*, 1305−1316.
(69) Araque, J. C.; Hettige, J. J.; Margulis, C. J. Modern Room Temperature Ionic Liquids, a Simple Guide to Understanding Their Structure and How It May Relate to Dynamics. *J. Phys. Chem. B* **2015**, *119*, 12727−12740.
(70) Guinier, A.; Fournet, G.; Yudowitch, K. L. *Small-Angle Scattering of X-Rays*; Wiley: New York, 1955.
(71) Pedersen, J. S. Determination of Size Distributions from Small-Angle Scattering Data for Systems with Effective Hard-Sphere Interactions. *J. Appl. Crystallogr.* **1994**, *27*, 595−608.

https://doi.org/10.1021/acs.macromol.2c02158
Macromolecules XXXX, XXX, XXX−XXX